Thin Solid Films 379 (2000) 122-127

Structural Characterization of ZrO2 Thin Films Produced via Self-Assembled Monolayer-Mediated Deposition Aqueous Dispersions

A.D. Polli[1], T. Wagner[1]*, A. Fischer[2], G. Weinberg[2], F.C. Jentoft[2], R. Schlögl[2] and M. Rühle[1]

[1]Max-Planck-Institut für Metallforschung, Seestraße 92, 70174 Stuttgart, Germany
[2]Department of Inorganic Chemistry, Fritz-Haber-Institute of the MPG, Faradayweg 4-6, 14195 Berlin, Germany

* Corresponding author: e-mail wagnerth@mf.mpi-stuttgart.mpg.de, phone +49-711-2095-466, fax +49-711-2095-120

Received 20 February 2000, accepted 31 August 2000

Abstract

Thin ZrO_2 films were produced at 323K by deposition of colloids from stable, aqueous dispersions (formed from 4mM $Zr(SO_4)_2$ in 0.4N HCl) onto silicon wafer-supported, functionalized self-assembled monolayers (SAMs). Deposition took place *without* visible bulk precipitation. As-deposited and heat-treated films were characterized by high-resolution transmission electron, analytical electron and scanning electron microscopy. In each case, an amorphous layer was found between the Si single crystal and the nanocrystalline ZrO_2 film. The amorphous layer of the as-deposited films was found to be composed of two distinct layers: SAM and SiO_2. Upon heat treatment at 773K for 2h in air or Ar, the SAM layer was no longer observed, suggesting that it decomposes and is removed completely in either atmosphere. The as-deposited films are tetragonal-ZrO_2 with a grain size of ~5nm throughout the film thickness. Following heat treatment, a slight increase in grain size was observed. Deposition without the SAM was also attempted, but failed to produce a strongly adherent, uniform film.

I. INTRODUCTION

ZrO_2 films are suitable as oxygen ion conductors for sensor (1,2) and fuel cell applications (3), as thermal barrier coatings for metal components (4), and nonabsorbing high refractive index coatings for optical applications (5,6). Moreover, sulfated ZrO_2 is a low temperature isomerization catalyst and nanocrystalline thin zirconia films may be used as a model system for investigation of the properties, particularly the acidity, of this catalyst (7,8). Inexpensive, scalable procedures for the preparation of zirconia films are required for their incorporation into industrial processes. One new processing route for thin oxide films that meets these criteria is the deposition from aqueous dispersions mediated by selected functional groups on the substrate surface. This method was introduced by Bunker et al. for the deposition of iron and calcium oxide films (9), and has been extended to form films of e.g. TiO_2 (10-14), ZrO_2 (13-16), ZrO_2-Y_2O_3 (15) and Y_2O_3 (17) on Si single crystals. The functional groups are the terminating groups of a self-assembled monolayer (SAM), i.e. an ordered array of long chain hydrocarbon molecules, which is attached to the substrate in a previous preparation step. The SAM-coated Si substrate is immersed into a deposition medium which is prepared by dissolving a metal salt. Although initially of clear appearance, these deposition solutions may age within hours to days in such a way that colloids are formed in the liquid phase, and these colloids may grow and agglomerate to give bulk precipitates. The aging process may take place before, after, and/or during the film growth.

For TiO_2, film growth has been observed for cases where the deposition medium remained visibly transparent (13); however, for ZrO_2, it has been

suggested that an unstable precipitating reaction medium is required for film growth to more than 3 nm thickness (14) and that film growth proceeds via the attachment of colloids (13, 15). Agarwal et al. (15) confirmed the existence of two phases in films produced from suspensions: nanocrystalline tetragonal (t-) ZrO_2, and amorphous basic zirconium sulfate. In these films, the zirconia particle size was inhomogeneous; a gradient perpendicular to the film surface was observed. Calcination in air was found to lead to complete conversion to nanocrystalline t-ZrO_2 (15).

The effect of solution chemistry and SAM termination on the film growth are currently the subject of much research (9, 12-15). For example, Fischer et al. (18) have investigated the role of large bulk precipitates on film morphology using scanning electron (SEM) and atomic force microscopy (AFM). They have shown that large particles can be removed from the film surface by washing, leaving behind generally undesirable large voids (18). Hence, one possibility to avoid the production of these large voids is to prevent the formation of large precipitates during growth. By varying reaction conditions, the formation of a suspension can be avoided and dispersions with nanoscale colloids may then remain stable for the time of the deposition (19). The goal of this work has been to elucidate the structural properties of the as-deposited and heat treated films produced from stable colloid dispersions. Specific emphasis on high-resolution transmission (HRTEM) and analytical electron microscopy (AEM) has been given.

II. Experimental Procedure

Preparation of the films followed closely the procedure of Agarwal et al. (15) and others (12, 13, 16); as such, only a brief outline of the process is given here. Slices (2x7mm) of a (100) p-type silicon wafer were cleaned sequentially in organic solvents and oxidizing Piranha solution (mixture of 70% H_2SO_4 : 30% H_2O_2) at 80°C. The SAM was then deposited by immersing the wafer into a solution of trichlorosilylhexadecane thioacetate (50 µl) in bicyclohexyl (5ml) for 5h. Following a chloroform rinse, the wafers were then immersed in the oxidizing agent oxone® (oversaturated aqueous solution of $2KHSO_5 * KHSO_4 * K_2SO_4$) for 5h in order to produce a sulfonic acid terminated SAM. The ZrO_2 films were then deposited from aqueous colloid dispersions which were prepared from 4mM zirconium sulfate solutions in 0.4N HCl. Immediately after preparation of these precursor solutions, the wafers were immersed and allowed to sit for 24h or 48h at 323K. The specimens were then removed from the deposition dispersion, rinsed with distilled water, and blown dry with argon under ambient conditions. In the procedure used here, bulk precipitation was not observed, although from analytical ultracentrifugation measurements (19), it is known that fine colloids with a mean diameter of ~1.7nm existed after 6, 12, and 24h. From these results, the reaction medium prepared at 323K is described as a stable colloid dispersion. It should be noted though that for deposition times greater than 24h, several needles where observed within the deposition cell. These needles were mm-sized and considered too large to be incorporated into the growing film. Thermal treatment of the films was performed in air or in 125ml/min argon for 2h at 773K (heating rate: 5K/min). Film growth was also attempted without a SAM, i.e. the SAM deposition step was omitted (oxone treatment included). The ZrO_2 film deposition without SAM was performed in two ways, (i) as described above and (ii) within 12h at 343K i.e. from an unstable medium undergoing bulk precipitation.

TEM samples were prepared following Strecker's method (20). HRTEM was performed on a JOEL 4000EX operated at 400keV. Electron spectroscopic imaging (ESI) was performed on a Zeiss EM 912 Omega energy filtering TEM operated at 120keV. The resulting elemental maps use inelastically scattered electrons to image the composition of a sample directly (21). SEM was performed with a Hitachi S-4000-FEG operated at 5keV.

III. Results and Discussion

Five sets of samples were investigated in this study. These include films deposited without SAM-mediation (*NoSAM*), those deposited under the conditions described above for 24h (*24hour*) and 48h (*48hour)*, and those deposited for 24h and later heat treated at 773K in an atmosphere of air (*Air*) or argon (*Ar*). As determined by

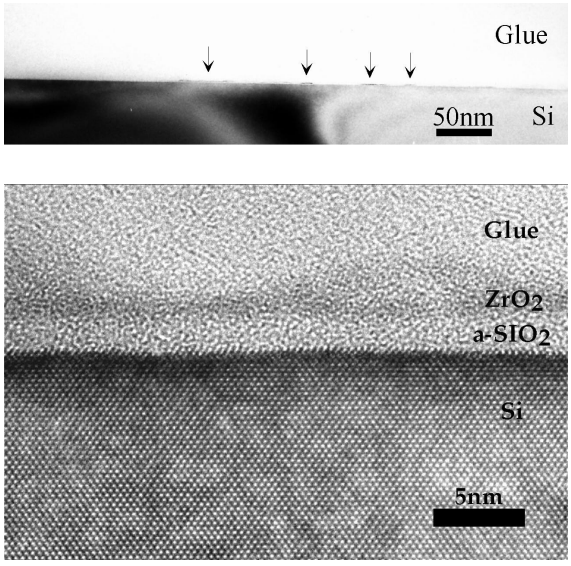

Figure1: (a) CTEM and (b) HRTEM image of NoSAM sample. Si-wafer was cleaned, oxidized, and directly treated with oxone, leaving the SAM-deposition step out. Deposition: 4mM Zr(SO4)2, 0.4N HCl, 323K, 24h.

HRTEM, each sample was composed of three distinct layers: single-crystal silicon, an amorphous layer, and a nanocrystalline zirconia thin film. Details of each are described in the following three sections.

A. Films without SAM.

Film growth was first attempted without SAM-mediation so that growth of ZrO_2 must occur directly on the chemically oxidized Si wafer. After 24h of film growth, cross-sectional CTEM images show, Figure 1a, that a uniform, continuous film could not be produced. Small isolated islands are observed, but the majority of the substrate is bare. HRTEM of these islands, as seen in Figure 1b, show that the islands are composed of only a < 2nm thick residue. The absence of lattice fringes within the image suggests that the material is noncrystalline, but the presence of zirconium was confirmed through energy dispersive X-ray spectroscopy (EDX). Within the bright-field image, the layer appears dark with respect to the amorphous (a-)SiO_2 due to its stronger Rutherford scattering (proportional to Z^2). Moreover, when deposition was carried out at 343K in a precipitating reaction medium, a continuous thin film could not be prepared. Figure 2 shows an SEM image taken from such a film following a washing procedure (18).

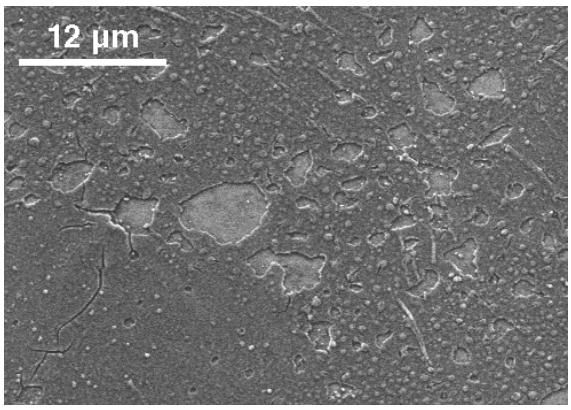

Figure 2: SEM image of film deposited at 343K from a precipitating reaction medium without SAM-mediation. The Si-wafer was cleaned, oxidized, and directly treated with oxone, leaving the SAM-deposition step out. Deposition: 4mM Zr(SO4)2, 0.4N HCl, 343K, 12h.

B. As-Deposited Films.

In contrast to the *NoSAM* sample, crystalline ZrO_2 films were readily observed in the *24hour* and *48hour* samples. SEM shows that after deposition for 24h a continuous thin film is prepared, Figure 3a. Cross-section analysis of the as-deposited films show that they are nanocrystalline t-ZrO_2, as seen in Figures 3b and 4. The majority of the lattice fringes within the film have a spacing of 0.30nm, consistent with the (101) d-spacing of t-ZrO_2. A summation of several fast Fourier transformations (FFTs) of the bright-field image from the *48hour* sample is shown in Figure 5a. This set of rings can be indexed like a powder selected-area electron diffraction pattern to reveal the structure of the nanocrystals. Toward this end, a rotationally-averaged profile of the FFT image in Figure 5a is shown in Figure 5b. A set of peaks is seen, each of which can be indexed to t-ZrO_2. Critical to distinguish t-ZrO_2 from cubic ZrO_2 is the weak (102) peak, unique to t-ZrO_2 and present in the figures, indicating that a significant amount of t-ZrO_2 exists. However, from this analysis it can not be excluded that some cubic ZrO_2 also exists within the film.

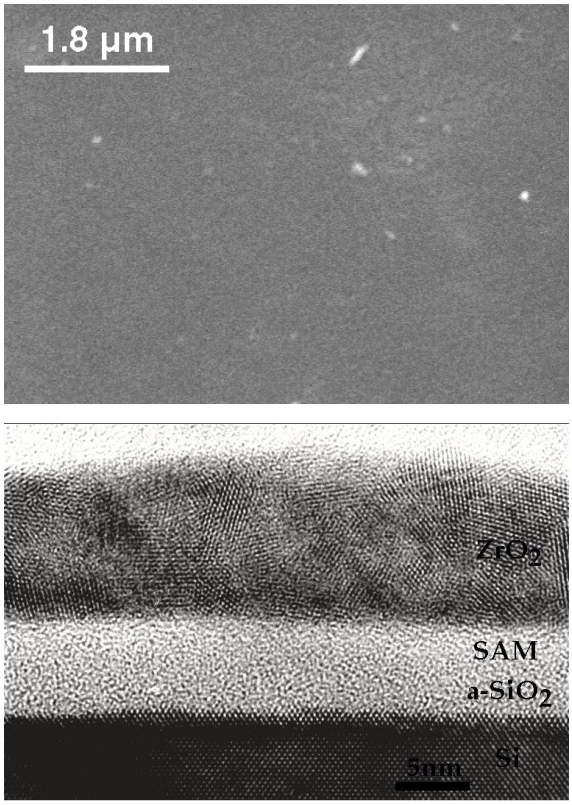

Figure 3: (a) SEM and (b) HRTEM image of the 24hour sample. Deposition: 4mM Zr(SO4)2, 0.4N HCl, 323K, 24h.

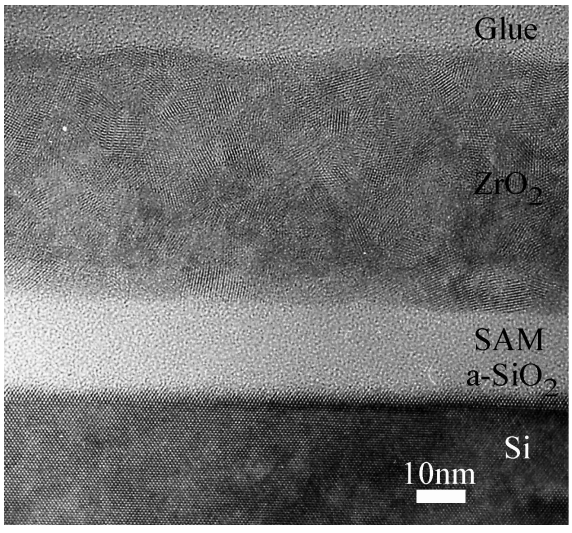

Figure 4: HRTEM image of 48hour sample. Deposition: 4mM Zr(SO4)2, 0.1N HCl, 323K, 48h.

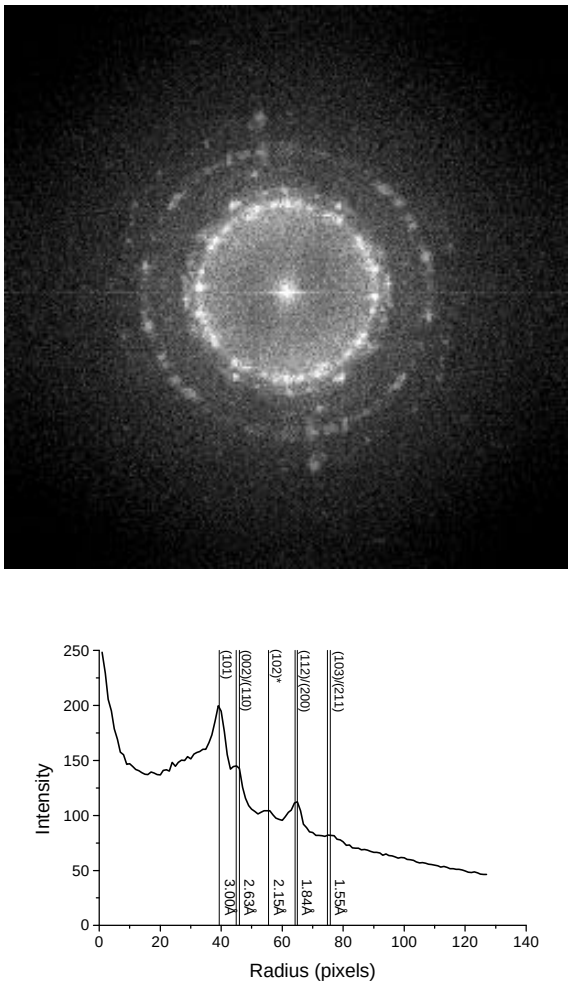

Figure 5: (a) Fast Fourier transformation and its (b) rotational-average profile for the HRTEM shown in Figure 4 from 48hour sample.

The grain size within each of the films is ~5nm. In the *48hour* sample with a film thickness of ~30nm, the grain size is also uniform, failing to show variation across the thickness of the film as has been observed by Agarwal et al. (15). Agarwal (15) investigated even thicker films (~125nm) and found ~10nm large particles close to the Si substrate (early stages of growth), and 2-3 nm large particles far away from the substrate. Although a gradient may not show because our films are thinner, we infer that the uniform grain size reflects the stable growth conditions which exist when bulk precipitation is avoided. The correlation between deposition conditions and film properties is further supported by the different zirconia grain sizes observed for early stages of growth, 10 nm (15) vs. 5 nm (this work). Also worth noting is the seemingly increasing, non-linear growth rate for the two deposition times studied; the film thickness for the *48hour* sample is roughly three times that of the *24hour* sample. This higher effective growth rate for the *48hour* sample could be indicative of a long incubation time for film growth. The formation of colloids within the precursor solutions may be expected to take a relatively longer time for conditions that do not lead to bulk precipitation as opposed to conditions in which bulk precipitation does occur, as have been typically employed (15).

Within the amorphous layer of the as-deposited films two distinct layers can be discerned. As illustrated in Figure 3b, the upper third of the amorphous layer appears brighter than the lower two thirds. This type of contrast is consistent with a structureless SAM layer on top of an a-SiO_2 layer. The lower average atomic number of the SAM (consisting of mainly C and H) would be expected to appear brighter in bright-field images due to weaker Rutherford scattering, the chief contrast mechanism in noncrystalline materials. This hypothesis is also supported by the expected thicknesses of the SAM and a-SiO_2 layers. Ellipsometry measurements on similar samples (13, 14, 22) suggest that a SAM thickness of ~2.2-2.5nm should be expected, while a SiO_2 thickness of roughly 2nm is routinely observed for silicon wafers following treatment with Piranha solution (22). Also, while the amorphous layer for the as-deposited films showed some variation in

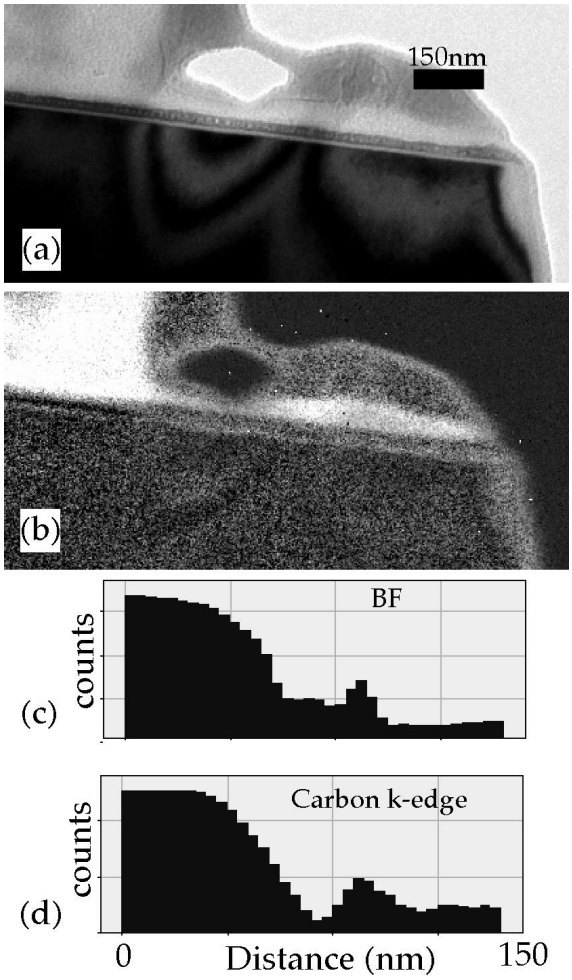

Figure 6: (a) Bright-field (BF) image and corresponding (b) carbon map collected by ESI from the 24hour sample. Profiles across the interface for the bright-field and carbon map are shown in (c) and (d), respectively.

thickness, it was always found to be greater than ~6nm, much thicker than that expected from oxidation in Piranha solution. A more direct observation of the SAM layer is shown in Figure 6 using ESI. Figures 6a and b show a bright-field image and the corresponding carbon map, respectively, of the *24hour* sample. Within the carbon map a bright strip is observed between the substrate and film. Section profiles across the interface are shown in Figures 6c and 6d. The small hump in the bright-field section profile (Figure 6c) is due to the amorphous layer. At the same position in the carbon map section profile (Figure 6d) an increase in carbon concentration is observed. The increase in carbon concentration within the amorphous layer is due to the presence of the SAM. It should be noted that due to the required large pixel size used during data collection and the physical properties of the detector (23), the represented width of the carbon-rich layer is much larger than that expected to exist within the sample.

C. Heat Treated Films.

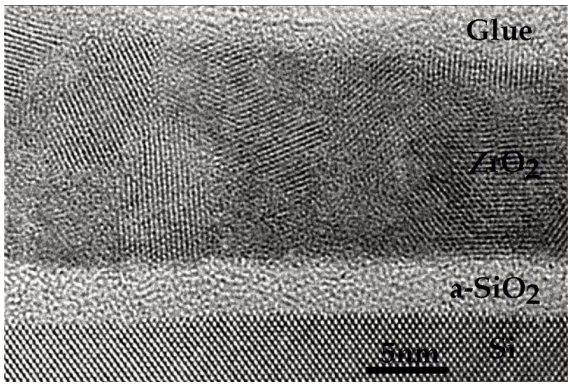

Figure 7: HRTEM image of Air sample. Deposition: 4mM Zr(SO4)2, 0.4N HCl, 323K, 24h. Annealing at 773K for 2h in air.

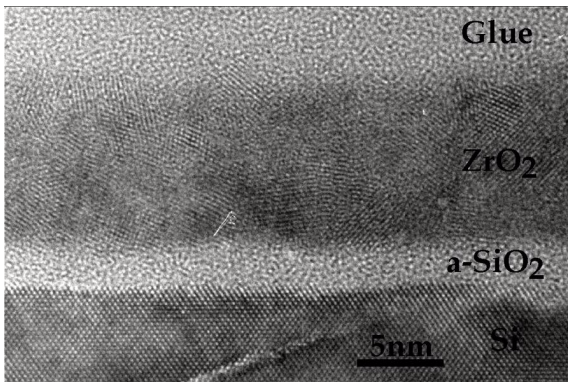

Figure 8: HRTEM image of Ar sample. Deposition: 4mmol Zr(SO4)2, 0.1N HCl, 323K, 24h. Annealing at 773K for 2h in 125ml/min argon.

The Air and Ar heat-treated films looked much like the as-deposited, except in regard to the amorphous layer thickness. The films were nanocrystalline, Figures 7 (*Air*) and 8 (*Ar*), with a grain size of approximately 5-8nm and a film thickness of ~11nm. In contrast though, the amorphous layers were consistently about 3nm in thickness— much less than that observed prior to heat treatment. Furthermore, no contrast originating from a possible SAM layer could be observed by HRTEM within the amorphous layer. These observations suggest that during heat treatment at 773K in either air or Ar, the SAM decomposes and is removed completely from the interface without disturbance of the thin film. Indeed, recent pyrolysis studies by Shin et al. (24) show that the pyrolysis of these particular SAMs is complete by 673K in air and initiated at 573-673K in N_2. Additionally, it should be noted that no significant decrease in adhesion between film and substrate was observed following burn-out of the SAM layer; both as-deposited and heat-treated samples failed to show delamination.

IV. CONCLUSIONS

Thin ZrO_2 films produced at 323K by SAM-mediated colloid deposition were shown to consist of nanocrystalline t-ZrO_2. The uniform grain size throughout the 11-30 nm thick film was attributable to growth in a stable colloid dispersion free of visible precipitates. Following deposition or heat treatment, each sample consisted of three distinct layers: silicon single crystal, an amorphous layer, and ZrO_2 film. HRTEM and AEM investigation showed that the amorphous layer of the as-deposited specimens consisted of both a SAM and an amorphous SiO_2 layer, while following heat treatment, no SAM could be observed, suggesting it could be removed without damaging the thin film. Growth without the SAM failed to produce an adherent, continuous thin film on oxidized silicon.

ACKNOWLEDGMENTS

The authors would like to thank Ute Salzberger and Maria Sycha for their TEM sample preparation work, Dr. Thomas Niesen for synthesis of the SAMs, and Dr. Joachim Mayer for help in acquiring the ESI images.

REFERENCES

1. M. Croset, P. Schnell and G. J. Valesco, Vac. Sci. Technol. **14**, 777 (1977).
2. Y. Miyahara, K. Tsukada and H. Miyagi, J. Appl. Phys. **63,** 2431 (1988).
3. N.J. Maskalick and C.C. Sun, J. Electrochem. Soc. **118,** 1386 (1971).
4. P.D. Harmsworth, R. Stevens, J. Mater. Res. **27**, 616 (1992).
5. K.V.S.R. Apparao, N.K. Sahoo and T.C. Bagchi, Thin Solid Films **129**, L71 (1985).
6. A. Duparré, E. Welsch, H.-G. Walther, N. Kaiser, H. Müller, E. Hacker, H. Lauth, J. Meyer and P. Weissbrodt, Thin Solid Films **187**, 275 (1990).
7. M. Hino, S. Kobayashi and K. Arata, J. Am. Chem. Soc. **101**, 6439 (1979).
8. X. Song and A. Sayari, Catal. Rev. **38**, 329 (1996).
9. B.C. Bunker, P.C. Rieke, B.J. Tarasevich, A.A. Campbell, G.E. Fryxell, G.L. Graff, L. Song, J. Liu, J.W. Virden and G.L. McVay, Science **264**, 48 (1994).
10. H. Shin, R.J. Collins, M.R. De Guire, A.H. Heuer and C.N. Sukenik, J. Mater. Res. **10**, 692 (1995).
11. R.J. Collins, H. Shin, M.R. De Guire, A.H. Heuer and C.N. Sukenik, Appl. Phys. Lett. **69**, 860 (1996).
12. H. Shin, M.R. De Guire and A.H. Heuer, J. Appl. Phys. **83**, 3311 (1998).
13. H. Shin, M. Agarwal, M.R. De Guire and A.H. Heuer, Acta mater. **46**, 801 (1998).
14. T.P. Niesen, M.R. De Guire, J. Bill, F. Aldinger, M. Rühle, A. Fischer, F. Jentoft and R. Schlögl, J. Mater. Res. **14**, 2464 (1999).
15. M. Agarwal, M.R. De Guire and A.H. Heuer, J. Am. Ceram. Soc. **80**, 2967 (1997).
16. M.R. De Guire, H. Shin, R. Collins, A. Agarwal, C.N. Sukenik and A.H. Heuer, Integrated Optics and Microstructures III, Massood Tabib-Azar, Editor., Proc. SPIE Z686, Vol. 2686, pp. 88-99 (1996).
17. M. Agarwal, M.R. De Guire and A.H. Heuer, Appl. Phys. Lett. **71**, 891 (1997).
18. A. Fischer, F.C. Jentoft, G. Weinberg, R. Schlögl, T.P. Niesen, J. Bill, F. Aldinger, M.R. De Guire and M. Rühle, J. Mater. Res. **14**, 3725 (1999).
19. H. Schnablegger , H. Cölfen, M. Antonietti, A. Fischer, F.C. Jentoft, G. Weinberg and R. Schlögl, in preparation.
20. A. Strecker, U. Salzberger and J. Mayer, Prakt. Metallogr. **30**, 482 (1993).
21. G. Dehm, F. Ernst, J. Mayer, G. Möbus, H. Müllejans, F. Phillipp, C. Sheu and M. Rühle, Z. Metallkd. **87**, 898 (1996).
22. R.J. Collins and C.N. Sukenik, Langmuir **11**, 2322 (1995).
23. A. Berger, J. Mayer and H. Kohl, Ultramicroscopy **55**, 10 (1994).
24. H. Shin, Y. Wang, U. Sampathkumaran, M.R. De Guire, A.H. Heuer and C. Sukenik, Mater. Res. **14**, 2116 (1999).